









Signatures of brain criticality unveiled by maximum entropy analysis across cortical states

Nastaran Lotfi ^{1,*} Antonio J. Fontenele ¹ Thaís Feliciano ¹ Leandro A. A. Aguiar ¹ Nivaldo A. P. de Vasconcelos ^{2,3}
 Carina Soares-Cunha ^{2,3} Bárbara Coimbra ^{2,3} Ana João Rodrigues ^{2,3} Nuno Sousa ^{2,3} Mauro Copelli ¹
 and Pedro V. Carelli ^{1,†}

¹*Departamento de Física, Universidade Federal de Pernambuco, Recife, PE 50670-901, Brazil*

²*Life and Health Sciences Research Institute (ICVS), School of Medicine, University of Minho, Braga, 4710-057, Portugal*

³*ICVS/3B's-PT Government Associate Laboratory, Braga/Guimarães, 4806-909, Portugal*



(Received 29 January 2020; accepted 1 July 2020; published 27 July 2020)

It has recently been reported that statistical signatures of brain criticality, obtained from distributions of neuronal avalanches, can depend on the cortical state. We revisit these claims with a completely different and independent approach, employing a maximum entropy model to test whether signatures of criticality appear in urethane-anesthetized rats. To account for the spontaneous variation of cortical states, we parse the time series and perform the maximum entropy analysis as a function of the variability of the population spiking activity. To compare data sets with different numbers of neurons, we define a normalized distance to criticality that takes into account the peak and width of the specific heat curve. We found a universal collapse of the normalized distance to criticality dependence on the cortical state, on an animal by animal basis. This indicates a universal dynamics and a critical point at an intermediate value of spiking variability.

DOI: [10.1103/PhysRevE.102.012408](https://doi.org/10.1103/PhysRevE.102.012408)

I. INTRODUCTION

Since Beggs and Plenz first reported neuronal avalanches in cortical slices [1], the critical brain hypothesis has gained support in experimental data and become an important paradigm in understanding brain dynamics [2–5]. According to this hypothesis, the computational advantages of a brain poised at or near a second-order phase transition are optimal transmission capacity [6], largest repertoire [4,7], and maximum dynamic range [8–10], among others.

In their seminal work, Beggs and Plenz have shown that the distribution of avalanche sizes in cultured slices of rat brain followed a power law with exponent $3/2$. This exponent coincides with the one found for a critical branching process (or any other model in the mean-field directed percolation universality class) [1,9]. This was just one of several scale-invariant phenomena expected to occur at a critical point.

In the years that followed, however, the investigation of neuronal avalanches in less reduced preparations raised some controversy. On one hand, power-law avalanche size distributions of spiking activity could be easily found *in vivo* during synchronized states [characterized by slow local field potential (LFP) oscillations] under ketamine-xylazine [11] and isoflurane [12] anesthesia. On the other hand, long-range time correlations could be observed only during desynchronized states (characterized by fast LFP oscillations) in freely behaving rats but not under ketamine-xylazine anesthesia [11].

Fontenele *et al.* have proposed a solution for the controversies between different data sets, by probing criticality across different cortical states [13]. It is well known that the degree of

synchronization in the brain varies with the behavioral state. In slow wave sleep, for instance, cortical LFP activity has low frequency and high amplitude, which corresponds to a synchronized state with high spiking variability. In an awake and attentive animal, cortical LFP has high frequency and low amplitude [14], corresponding to a desynchronized state with low spiking variability. Fontenele *et al.* have identified consistent markers of a phase transition at an intermediate level of spiking variability, where both avalanches and time correlations consistently satisfy more stringent scaling relations [13,15,16].

Here we investigate whether a similarly spike-variability-dependent analysis of neuronal data would reveal signatures of criticality under a completely different approach. We focus on maximum entropy models [17], which consist of a methodology of extracting the desired statistics from limited data with a minimum of plausible assumptions. Bialek and collaborators have shown that maximum entropy models are an effective and parsimonious way of reconstructing higher-order statistics in neuronal dynamics, based on single-neuron firing rates and pairwise correlations [18]. Later, other works have proposed that signatures of criticality could be unveiled in retinal data using the divergence of a generalized specific heat of the maximum entropy model built from the data [19,20].

Specifically, we use a maximum entropy model which is based on the firing rate of the network in different time steps [20] to study criticality across cortical states in urethane-anesthetized rats. As done previously, here a cortical state will be characterized by a proxy, namely, the coefficient of variation (CV) of the population firing rate [13,21–24]. We divide the time series according to CV values and apply the maximum entropy method for each division, analyzing the

*nastaran@df.ufpe.br

†pedro.carelli@ufpe.br

family of specific heat curves as the urethanized brain drifts from more synchronous to less synchronous states.

II. METHODS

A. Data acquisition

The data used in this analysis are taken from two experimental setups. As has been described previously [13], three Long-Evans rats, male, 250–360 g, 3–4 mo old (five Wistar-Han rats, male, 350–500 g, 3–6 mo old, Charles River) were used in the recordings. Animals were anaesthetized with 1.58 g/kg (1.44 g/kg) of fresh urethane, diluted at 20% in saline, in three injections (i.p.), 15 min apart.

We implanted 32- (64-)channel silicon probes (Buzsaki-A32/BuzsakiA64sp, Neuronexus), which are composed of four (six) shanks with eight (10) sites/shank with impedance of 1–3 Mohm at 1 kHz, in the primary visual cortex of the rats (V1, Bregma: AP = −7.2, ML = 3.5). Shanks were 200 μm apart, and the area of each site was 160 μm², disposed from the tip in a staggered configuration, 20 μm apart. All data were sampled at 24 (30) kHz, amplified and digitized in a PZ2 TDT, which transmits to a RZ2 TDT base station (amplified and digitized in a single head-stage Intan RHD2164). All recordings were analyzed up to a duration of 3 h.

After recordings, spike sorting was performed using the Klusta-Team software [25,26] on raw electrophysiological data. Housing, surgical, and recording procedures were in strict accordance with the CONCEA-MCTI and were approved by the Federal University of Pernambuco (UFPE) Committee for Ethics in Animal Experimentation (23076.030111/2013-95 and 12/2015) and European regulations (European Union Directive 2010/63/EU).

B. Maximum entropy analysis

From the data we extracted the binary spiking matrix $\{s_{i,t}\}$ as follows: we divided the time series into windows of length Δt (20–50 ms). If neuron i has spiked at least once in a time window t , then $s_{i,t} = 1$ (otherwise, it is zero). In Appendix D (Fig. 9) we show that the results are robust with respect to the value of Δt .

Since we want to address the differences in dynamical regimes observed in different cortical states, it is natural to employ a variant of the maximum entropy formalism that takes into account the dynamical nature of the spike trains. Following Mora *et al.* [20], a Boltzmann-like distribution is defined,

$$P_\beta(s_{i,t}) = \frac{1}{Z(\beta)} \exp[-\beta E(\{s_{i,t}\})], \quad (1)$$

where $Z(\beta)$ is the normalization constant, E is the “energy” of the spike trains, and $\beta \equiv 1/T$, a control parameter, is equivalent to an inverse temperature T and it is set to 1 to describe the observed spike statistics. The idea of the method is to maximize the entropy

$$H_\beta = - \sum_{\{s_{i,t}\}} P(\{s_{i,t}\}) \log P(\{s_{i,t}\}) \quad (2)$$

subject to observable constraints in the data [17,18].

Being interested only in global phenomena and not in individual interaction between neurons, Mora *et al.* proposed a maximum entropy model where the energy function depends only on the population firing rates and transitions between consecutive firing rates [20]. In this way, the joint probability distributions of $K_t \equiv \sum_{i=1}^N s_{i,t}$ at two different times $P_u(K_t, K_{t+u})$ are constrained, and the energy function is defined as

$$E = - \sum_t h(K_t) - \sum_t \sum_{u=1}^v J_u(K_t, K_{t+u}), \quad (3)$$

where N is the number of neurons, L is the number of time bins, and $v \geq 1$ is the temporal range of model.

The fitting of the model consists in solving the inverse problem of finding $h(K)$ and $J_u(K, K')$ such that $P_{u,\text{model}}$ predicted by the model corresponds to $P_{u,\text{data}}$ obtained from the data. While $P_{u,\text{data}}$ is directly estimated from the spike trains, $P_{u,\text{model}}$ is calculated via the technique of transfer matrices (see Ref. [20] for details). The model learning is performed by an iterative process based on the difference between the probabilities predicted from the model and the probabilities from the data:

$$h(K_t) \leftarrow h(K_t) + \epsilon [P_{\text{data}}(K_t) - P_{\text{model}}(K_t)], \quad (4)$$

$$J_u(K_t, K_{t+u}) \leftarrow J_u(K_t, K_{t+u}) + \epsilon [P_{u,\text{data}}(K_t, K_{t+u}) - P_{u,\text{model}}(K_t, K_{t+u})], \quad (5)$$

which is equivalent to a gradient descent on the log-likelihood [20]. Choosing a small enough value of ϵ ensures the convergence of $h(K)$ and $J_u(K_t, K_{t+u})$.

Once P_β is determined, the specific heat can be calculated as a function of β :

$$c(\beta) = \frac{\beta^2}{NL} \langle \delta E^2 \rangle_\beta, \quad (6)$$

where $\delta E \equiv E - \langle E \rangle_\beta$ is the fluctuation from the mean energy and its average is taken under P_β [20]. Note that P_β maximizes the entropy given the data only for $\beta = 1$. By allowing T to vary, a family of probability distributions is traversed, and a peak of c that tends towards $T = 1$ as N increases is interpreted as a signature that the system is critical [19,20].

In order to handle the dependence of c on the system size, for each data set N neurons were selected randomly from the total set of neurons recorded. This was repeated over 20 random selection of units, and the shown result is their average. To control for the significance of the results, we also repeat the specific heat calculation for surrogate data, in which for each neuron the sequence of interspike intervals was shuffled (Appendix A).

C. CV parsing

To understand how the spiking variability could affect the maximum entropy analysis, the data are segmented in windows of duration $W = 10$ s. For each window j , the coefficient of variation (CV) of the population firing rate K_t is calculated:

$$\text{CV}_j = \frac{\sigma_j}{\mu_j}, \quad (7)$$

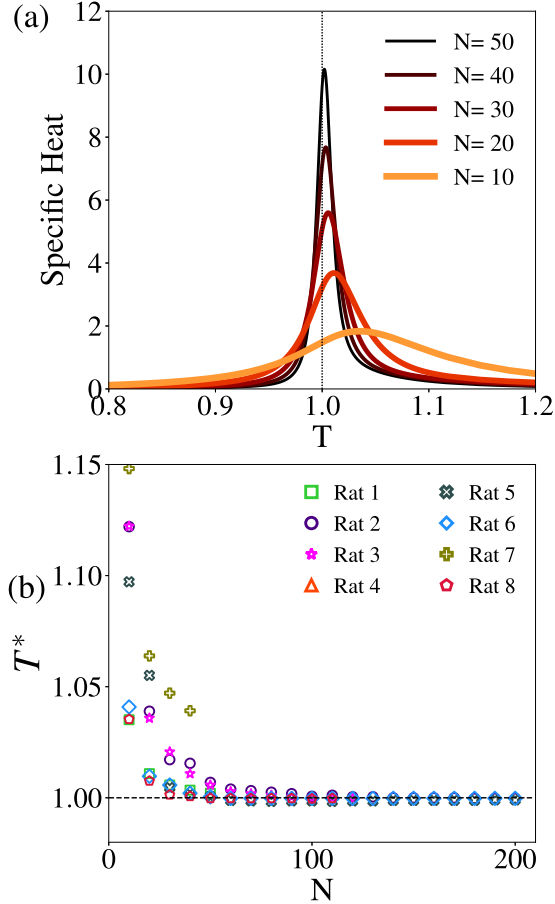


FIG. 1. (a) Specific heat versus temperature (T) for an increasing number of neurons (rat 1, which had 52 neurons recorded), with $\Delta t = 20$ ms and $v = 2$. (b) Variation of critical temperature (T^*) as a function of the number of neurons (N) considered to fit the model.

where μ_j is the mean and σ_j is the standard deviation of K_i within window j . To have better statistics for the model fitting, we concatenate 50 windows of similar CVs, calculate their average $\langle CV \rangle$, and run the maximum entropy algorithm to find the heat capacity as a function of the temperature for different values of $\langle CV \rangle$. Robustness of the results against changes in W was also verified (Appendix D, Fig. 11). Note that CV increases monotonically with the average pairwise spiking correlation (Appendix B, Fig. 7), which is a well-established marker of cortical states [23].

III. RESULTS

A. Analysis of the time series as a whole

We start our investigation by simply considering the whole time series of the data sets. Fitting the maximum entropy model to the data, we obtained curves of specific heat $c(T)$. T^* is defined as the temperature at which c is maximal. As we exemplify in Fig. 1(a) for a single rat, the larger the number N of neurons, the closer T^* was to $T = 1$ and the larger the value of $c(T^*)$, suggesting a critical dynamics [19,20]. These results are consistent across rats, as shown in Fig. 1(b). When we repeat the analysis for surrogate (shuffled) data, the specific heat values are much smaller and the peaks

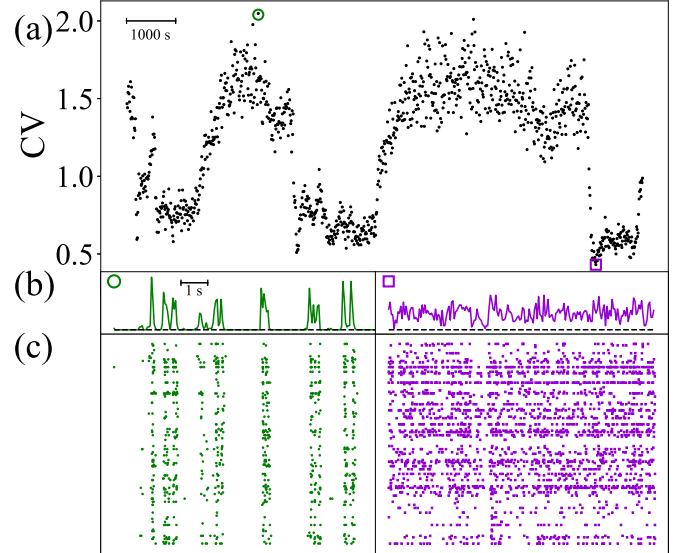


FIG. 2. (a) CV as a function of time for the whole time series (rat 3) ($\Delta t = 50$ ms, $W = 10$ s). The maximum and minimum values are highlighted with a circle and a square, respectively. (b) Firing rate K_i corresponding to the maximum (left) and minimum (right) CV values of the time series (dashed line is an indicator of zero). (c) Raster plots corresponding to (b), where each line represents a different neuron and each dot is a spike. Larger (smaller) values of CV correspond to more (less) synchronized states.

occur for temperatures $T_{\text{surrogate}}^* < 1$ [Appendix A, Fig. 6(a)]. This suggests that surrogate data at $T = 1$ are above the critical temperature, and therefore in a disordered phase (as expected).

B. Analysis by spiking variability

These results, however, should be taken with a grain of salt. Note that the model proposed by Mora *et al.* assumes that the data are stationary [20], since the parameters h and J_{ii} in the energy function of Eq. (3) are time independent. But the dynamics of the spiking data in urethanized brains, on the other hand, changes considerably in the timescale of the whole record ($\sim 2-3$ h). A common index to quantify these changes is the coefficient of variation (CV) of the population firing rate, which we calculate within windows of duration W . Figure 2(a) shows the time evolution of CV for a single rat on the scale of hours, where one observes instances of very high spiking variability in more synchronized states [$CV \simeq 2$, left plots of Figs. 2(b) and 2(c)], very low spiking variability in more desynchronized states [$CV \simeq 0.5$, right plots of Figs. 2(b) and 2(c)], and pretty much everything in between. As shown in Appendix C (Fig. 8), each experiment has its own, apparently unpredictable, evolution of $CV(t)$.

This lack of stationarity on longer timescales suggests that we are mixing together very different dynamical regimes when the maximum entropy analysis is applied to the whole time series. To reconcile the assumed hypothesis of stationarity of the model and the changes in cortical state in a slow $O(> 10$ s) timescale, we consider this analysis by previously segmenting and aggregating data by CV values, in line with Fontenele *et al.* [13]. Once we have selected the epochs of data

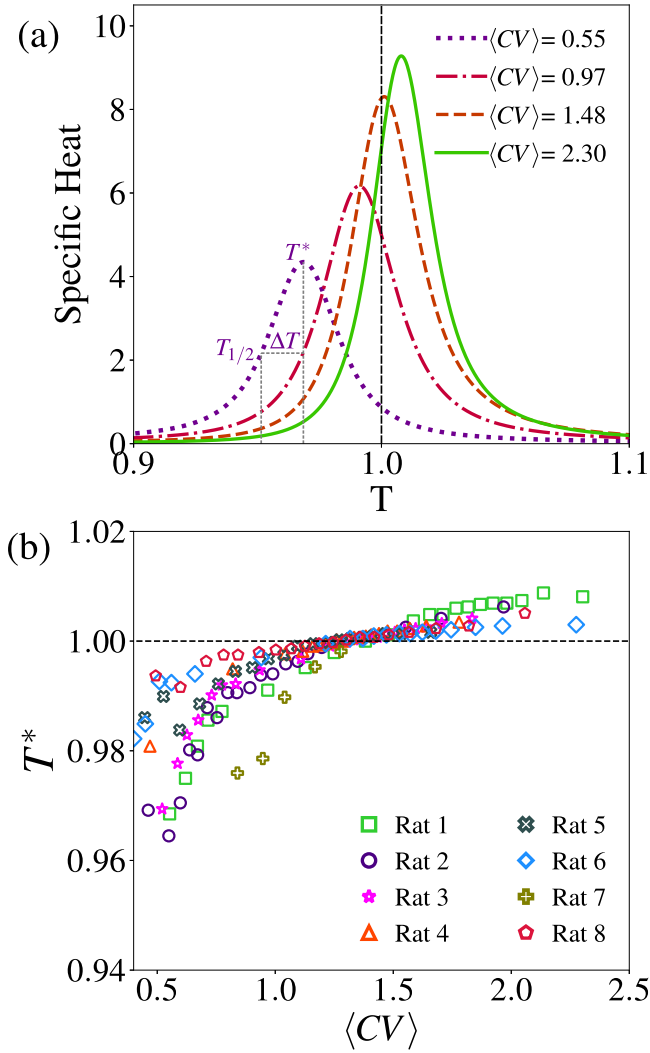


FIG. 3. (a) Specific heat as a function of the temperature for different values of $\langle CV \rangle$ of rat 1, $N = 52$, $\Delta t = 50$ ms). The definitions of ΔT [Eq. (8)], T^* and $T_{1/2}$ are illustrated for $\langle CV \rangle = 0.55$ (see text for details). (b) T^* versus $\langle CV \rangle$ for different rats, where we have employed the maximal number of neurons in each data set.

parsed by $\langle CV \rangle$ that will feed the maximum entropy model, the fitting is identical to what has been previously described [20], and for each $\langle CV \rangle$ the model fitting is independent from the others.

To do so, the maximum number of neurons in each data set is considered. In Fig. 3(a) the dependence of $c(T)$ with $\langle CV \rangle$ is shown for one data set [rat 1; results for surrogate data are shown in Appendix A, Fig. 6(b)]. As the value of $\langle CV \rangle$ increases, the temperatures T^* of the specific heat peak now increase from below $T = 1$ to above it.

The interpretation of these results can be tricky. Note that the data are, by definition, described by the model at $T = 1$. Whether $T = 1$ is considered “high” or “low,” i.e., whether the data correspond respectively to a disordered or an ordered phase, depends on where the critical temperature T^* lies. For low $\langle CV \rangle$ (desynchronized states), $T = 1$ is higher than T^* , suggesting a disordered phase. Accordingly, the high- $\langle CV \rangle$ (synchronized states) would correspond to an ordered phase.

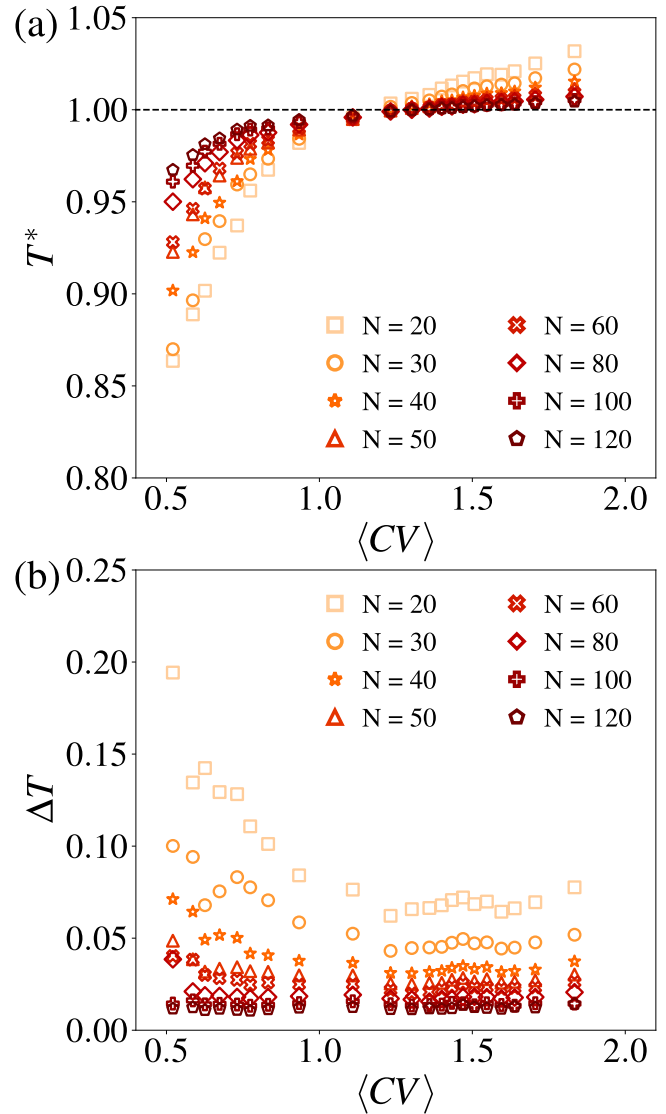


FIG. 4. (a) Temperature T^* of the specific heat peak versus $\langle CV \rangle$ for different numbers of neurons (rat 3, $\Delta t = 50$ ms). Note that T^* approaches $T = 1$ from below (above) for low (high) $\langle CV \rangle$. (b) Width ΔT [see Eq. (8) and Fig. 5(a)] of the specific heat curve versus $\langle CV \rangle$ for different numbers of neurons.

Therefore, if we parse the data by spiking variability, the signatures of criticality do not appear in the whole time series. As shown in Fig. 3(b), T^* coincides with $T = 1$ only in a narrow range of $\langle CV \rangle$. These results are robust across animals and suggest a critical point between the desynchronized and the synchronized extremes, as reported by Fontenele *et al.* [13].

Of course, different rats have different numbers of recorded neurons, and we would like to understand whether those differences can be controlled for when analyzing the $\langle CV \rangle$ dependence of $c(T)$ curves, such as those of Fig. 3(a).

On the one hand, as we show in Fig. 4(a), T^* gets increasingly closer to $T = 1$ for *any* value of $\langle CV \rangle$ as the number of neurons increases (while the point with $T^* \simeq 1$ remains relatively N -independent). On the other hand, this increasing proximity between T^* and $T = 1$ should be interpreted with

caution. Whether $T^* - 1$ is small or large depends on a comparison with some natural scale of temperature variation in the problem.

We propose to compare $T^* - 1$ with the width ΔT of the bell-shaped $c(T)$ curve at half height,

$$\Delta T \equiv T^* - T_{1/2}, \quad (8)$$

where $T_{1/2}$ is defined by $c(T_{1/2}) = c(T^*)/2$, as shown in Fig. 3(a). Figure 4(b) shows that the $c(T)$ curves become sharper as N increases, thus providing a natural scale with which to compare the results in Fig. 4(a). We thus define a *normalized distance to criticality* τ , defined as

$$\tau \equiv \frac{T^* - 1}{\Delta T}. \quad (9)$$

Differently from the behavior of $T^* - 1$ (Fig. 4), τ as a function of $\langle CV \rangle$ converges quickly to a well-behaved function even for a fraction of the total number of neurons [Fig. 5(a)]. Note that both axes of this curve are dimensionless. Besides, this function $\tau(\langle CV \rangle)$ seems to be universal for this setup, in the sense that it is reproduced by different rats with different numbers of neurons [Fig. 5(b)]. In particular, for all rats, τ crosses zero in approximately the same critical value of $\langle CV \rangle^* \approx 1.28 \pm 0.08$. This crossing is a strong indicator of universal behavior segregating regimes of low temperatures (synchronized states) and high temperatures (desynchronized states).

Naturally, the next natural step would be to extend this analysis to nonanesthetized animals. These recordings, however, are more difficult to obtain and more susceptible to noise. We used publicly available cortical recordings of mice [27]. The results of this analysis are shown in Fig. 5(b) and suggest that, as CV increases, $|\tau|$ of freely behaving mice decreases (following a similar trend to data of anesthetized rats) but stops short of reaching the critical point. There is, however, a serious limitation in the interpretation of these results, or at least in the direct comparison with the anaesthetized rat data. While rats were implanted with six-shank silicon probes recording around the same cortical layer, mice data were recorded with a single-shank probe which recorded across cortical layers. It is unclear at this point how much this difference could influence the results, and interpretations should carefully take this into account. In our view, therefore, the question whether or not the awake cortex is critical remains under debate.

IV. CONCLUSION

In conclusion, we have applied the maximum entropy approach of Mora *et al.*, which takes into account the dynamical aspects of networks activity, to cortical spiking data of urethane-anesthetized rats. Since spiking variability undergoes major changes along the hours of the experiments, the data sets were parsed by $\langle CV \rangle$ in an attempt to fulfill, for each $\langle CV \rangle$, the stationarity required by the model.

When analyzed in this way, the method reveals signatures of criticality for a very narrow range of $\langle CV \rangle$ values. For very low (high) $\langle CV \rangle$, the system is more desynchronized (synchronized), which corresponds to a disordered (ordered) phase, i.e., with $T = 1 > T^*$ ($T = 1 < T^*$). We introduced

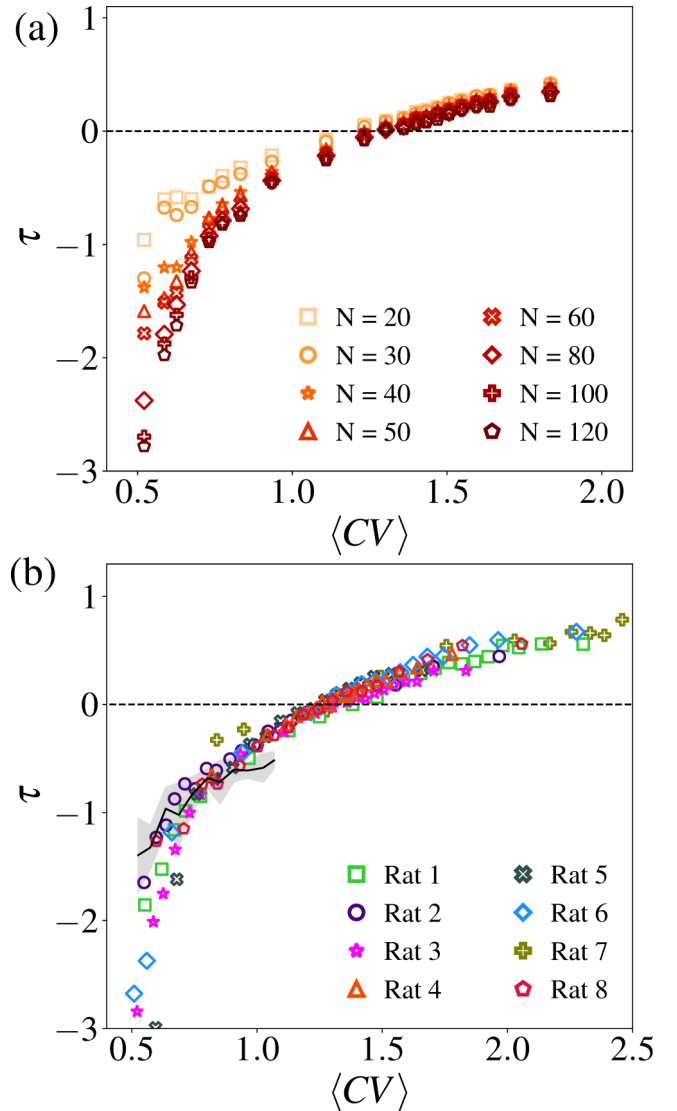


FIG. 5. (a) Normalized distance to criticality τ versus $\langle CV \rangle$ quickly converges to a well-behaved function for increasing N (rat 3, $N = 130$, $\Delta t = 50$ ms). (b) τ versus $\langle CV \rangle$ for the maximum number of neurons in each data set. τ crosses zero at approximately the same value of $\langle CV \rangle$ for all rats (see text for details). Results for nonanesthetized mice ($n = 10$) are shown with a solid line (average) and shading (standard deviation).

a normalized distance to criticality τ whose behavior was universal across rats, consistently crossing zero at the same critical value $\langle CV \rangle^*$. These results are not reproduced by shuffled data and, as shown in Appendix D, stand robust against changes in the time bin Δt used to calculate firing rates (Fig. 9), the order ν of the model (Fig. 10), and the width W of the windows employed to calculate CV (Fig. 11).

The critical value $\langle CV \rangle^*$ obtained with the maximum entropy approach is compatible (within error bars) with the one obtained by Fontenele *et al.* ($\langle CV \rangle^* \approx 1.4 \pm 0.2$) via neuronal avalanche scaling analysis [13]. Despite the completely different nature of these two approaches, both strongly suggest that a phase transition occurs at an intermediate level of synchronization for urethane-anesthetized rats.

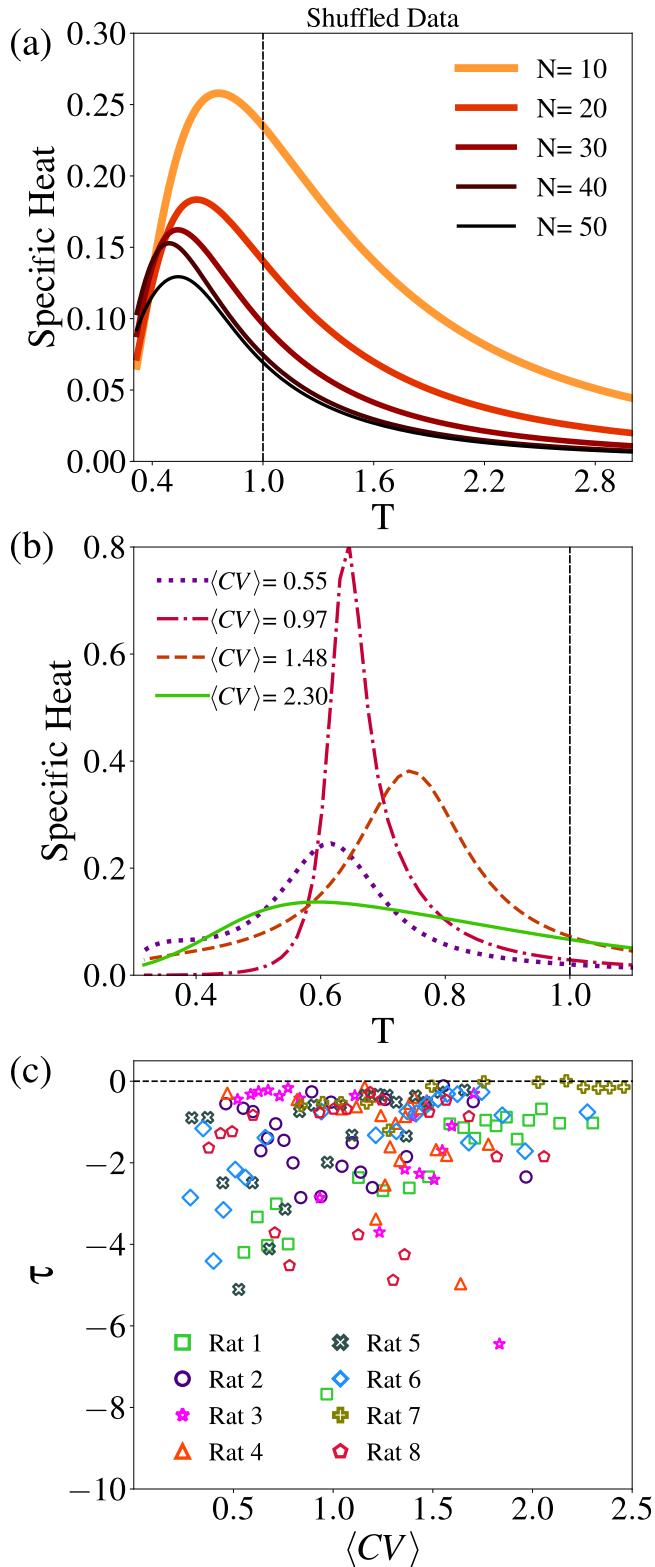


FIG. 6. Variation of specific heat for shuffled data of rat 1 ($\Delta t = 50$ ms). (a) Results for the whole time series with different numbers of neurons. (b) We illustrate the influence of $\langle CV \rangle$ on the specific heat for a few examples with the maximum number of neurons. (c) We show a scatter plot of normalized distance to criticality τ versus $\langle CV \rangle$ for all rats, breaking the universal structure shown in Fig. 11(b). In (b) and (c), the value of CV was calculated for the original (nonshuffled) time series.

ACKNOWLEDGMENTS

We acknowledge Thierry Mora and Olivier Marre for sharing the maximum entropy analysis code and fruitful discussions. N.L. is thankful to FACEPE (Grant No. BCT-0426-1.05/18) and CAPES (Grant No. 88887.308754/2018-00) for their support. M.C. and P.V.C. acknowledge support from CAPES (PROEX 534/2018 Grant No. 23038.003382/2018-39), FACEPE (Grant No. APQ-0642-1.05/18), CNPq (Grants No. 301744/2018-1 and No. 425329/2018-6), and Universidade Federal de Pernambuco (UFPE). This article was produced as part of the activities of the FAPESP Center for Neuromathematics (Grant No. 2013/07699-0, S. Paulo Research Foundation). C.S.-C. and B.C. acknowledge support from FCT (Grants No. SFRH/BD/51992/2012 and No. SFRH/BD/98675/2013) and PAC, MEDPERSYST Project POCI-01-0145-FEDER-016428 (Portugal 2020). A.J.R. received support from an FCT Investigator Fellow (IF/00883/2013) and acknowledges support from the Janssen Neuroscience Prize (first edition) and the BIAL Grant No. 30/2016.

APPENDIX A: SURROGATE DATA

To test the significance of our results presented in the main text, we repeated the analysis over surrogate data. To obtain these series each neuron spike timing was randomized, keeping the total number of events fixed.

In the whole time series of the shuffled data sets, we verify that the specific heat remains with small values and its peak declines when the number of neurons increases, in opposition to the increase of specific heat of the original spiking series [compare Fig. 6(a) and Fig. 1(a)]. Also, the specific heat peak for shuffled data is typically very far from $T = 1$ [Fig. 6(a)].

Repeating the maximum entropy analysis as a function of the cortical state ($\langle CV \rangle$) for surrogate data, we verify

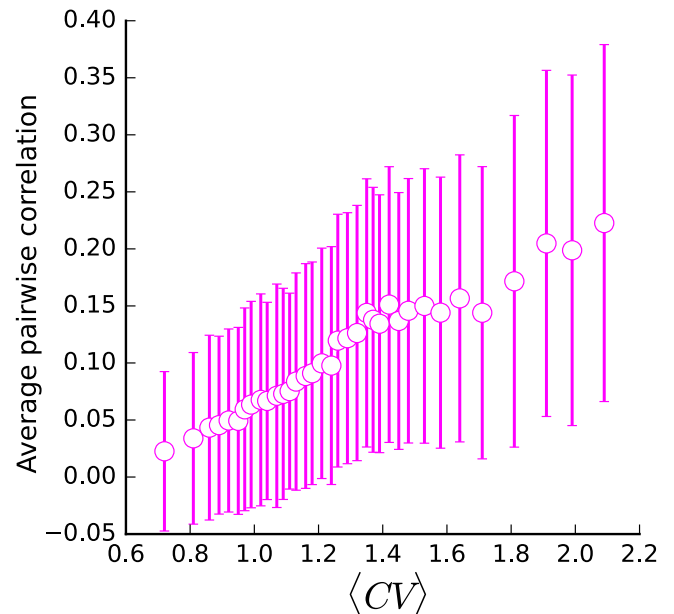


FIG. 7. Pairwise spiking correlation (symbols are averages over pairs of 138 neurons; error bars are standard deviations) as a function of CV for a single urethane-anesthetized rat.

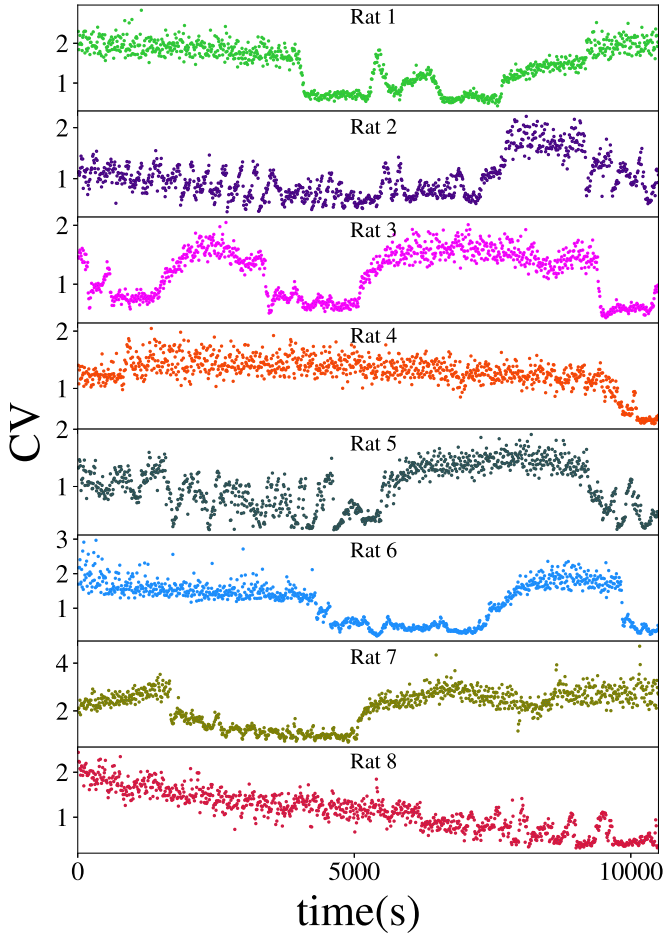


FIG. 8. Time series of CV for different recordings ($\Delta t = 50$ ms, $W = 10$ s).

that there is no specific trend in the behavior of the specific heat [Fig. 6(b), in comparison to Fig. 3(a)]. To emphasize the inconsistency of the shuffled data behavior, we show in Fig. 6(c) the surrogate analysis of τ for all data sets. This plot shows that the universal trend in Fig. 3(b) disappears when the data are randomized. It is important to mention that in Figs. 6(b) and 6(c) the values of CV were calculated on the original time series (before shuffling). The CV for the shuffled time series is flat, with an average 0.35 and standard deviation 0.08.

APPENDIX B: RELATION BETWEEN CV AND PAIRWISE CORRELATIONS

Cortical states at the scale of spikes are characterized by the distribution of pairwise spiking correlations: desynchronized states have a pairwise correlation distributed around a near-zero mean, whereas synchronized states have positive correlations on average [23]. In Fig. 7 we show the average and standard deviation of pairwise spiking correlations of a single animal along the whole range of CV values. The monotonic (almost linear) dependence reinforces CV as a convenient proxy for cortical states.

We quantified pairwise spiking correlations based on spike trains of single-unit activity. Initially, for each cell i we obtain

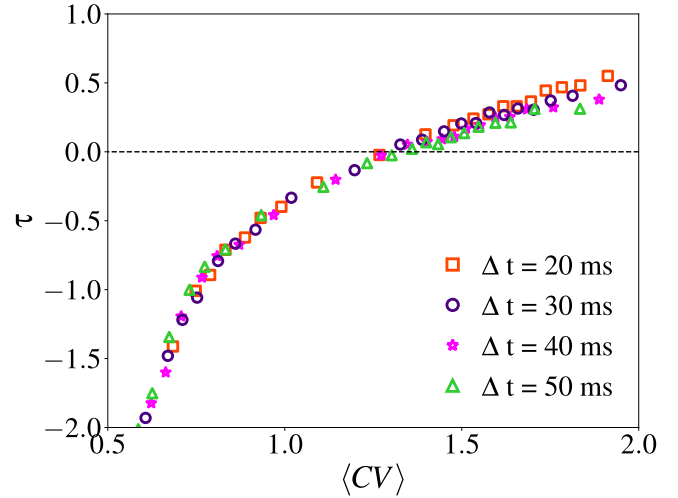


FIG. 9. Robustness of the behavior of normalized distance to criticality (τ) versus $\langle CV \rangle$, considering different time bins (Δt) for calculating firing rates ($W = 10$ s and $v = 2$).

a spike count time series r_i at millisecond resolution ($\Delta t = 1$ ms). Subsequently, in order to specify the timescale on which the spiking correlation is calculated, we convolved each time series r_i with a kernel h :

$$n_i(t) = h_{s_1, s_2}(t) * r_i(t), \quad (\text{B1})$$

where h is a Mexican-hat kernel obtained by the difference between two zero-mean Gaussians with standard deviations $s_1 = 100$ ms and $s_2 = 400$ ms [22]. The spiking correlation coefficient ρ_{ij} between two units i and j is then given by

$$\rho_{ij} = \frac{\text{Cov}(n_i, n_j)}{\sqrt{\text{Var}(n_i)\text{Var}(n_j)}}, \quad (\text{B2})$$

where Var and Cov are the variance and covariance, respectively.

APPENDIX C: CV TIME SERIES

In Fig. 8 we show CV time series of the ~ 3 -h-long continuous recordings for different rats. It can be seen that, for all rats, there are variations from low to high values of CV. This illustrates that, on a timescale of hours, we can have important changes in the cortical states even for anesthetized preparations [21].

APPENDIX D: ROBUSTNESS OF THE RESULTS

To further probe the robustness of our results, we also repeated our analysis with different timescales for discretization of the neural firing and parsing the cortical states.

1. Time resolution for the firing rates

The first temporal parameter we have modified was the resolution, Δt , used in the calculation of the firing rates. In Fig. 9 different values are selected for Δt , and maximum entropy analysis is done with variation of $\langle CV \rangle$. On the one hand, Δt must be large enough to ensure that the firing rate

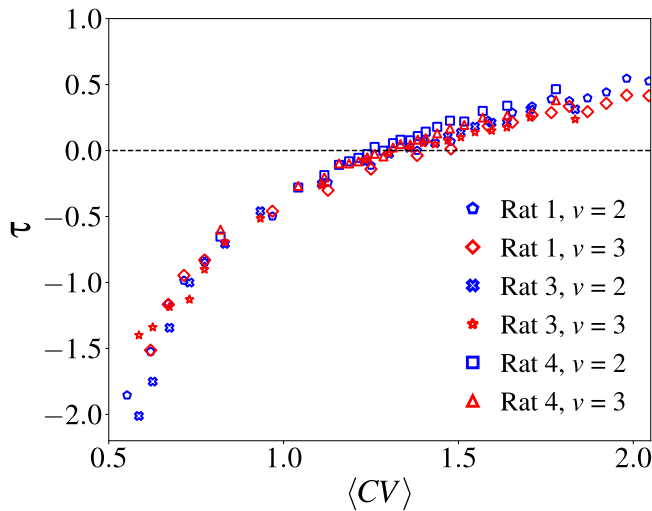


FIG. 10. Robustness of the behavior of the normalized distance to criticality (τ) as a function of $\langle CV \rangle$ for different values of the model order (ν). We show results from three typical rats using $\nu = 2$ and $\nu = 3$ ($\Delta t = 50$ ms and $W = 10$ s).

of the population is well characterized. On the other hand, it should not be so large that it averages away important population dynamics. Also, if Δt is too large, many spikes would be counted as a single one. Any analysis using Δt on the order of tens of milliseconds satisfies these constraints. Figure 9 shows that all curves collapse, and, therefore, results do not depend on a fine-tuned time window.

2. Model order ν

Another parameter of the model is its temporal order ν , which defines how many time steps are considered for the

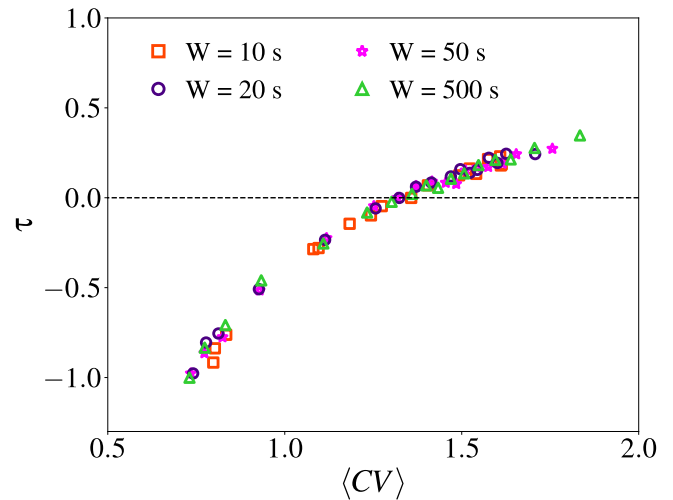


FIG. 11. Universal behavior of normalized distance to criticality (τ) versus $\langle CV \rangle$ for different timescales used for calculating CV ($\nu = 2$ and $\Delta t = 50$ ms).

model dynamics [see Eq. (3)]. We show in Fig. 10 (with data from three randomly selected rats) that the curves $\tau(\langle CV \rangle)$ for model orders $\nu = 2$ and 3 are very similar.

3. Time resolution for defining a cortical state

We have also explored different values for the timescale used to define a cortical state. In the results shown in the main text, a time window of $W = 10$ s was used for calculating CV. Figure 11 shows that changing this parameter in the analysis does not affect the results for the normalized distance to criticality.

-
- [1] J. M. Beggs and D. Plenz, Neuronal avalanches in neocortical circuits, *J. Neurosci.* **23**, 11167 (2003).
 - [2] J. M. Beggs, The criticality hypothesis: How local cortical networks might optimize information processing, *Philos. Trans. R. Soc. A* **366**, 329 (2007).
 - [3] D. R. Chialvo, Emergent complex neural dynamics, *Nat. Phys.* **6**, 744 (2010).
 - [4] W. L. Shew and D. Plenz, The functional benefits of criticality in the cortex, *Neuroscientist* **19**, 88 (2013).
 - [5] S. di Santo, P. Villegas, R. Burioni, and M. A. Muñoz, Landau–Ginzburg theory of cortex dynamics: Scale-free avalanches emerge at the edge of synchronization, *Proc. Natl. Acad. Sci. USA* **115**, E1356 (2018).
 - [6] W. L. Shew, H. Yang, S. Yu, R. Roy, and D. Plenz, Information capacity and transmission are maximized in balanced cortical networks with neuronal avalanches, *J. Neurosci.* **31**, 55 (2011).
 - [7] C. Haldeman and J. M. Beggs, Critical Branching Captures Activity in Living Neural Networks and Maximizes the Number of Metastable States, *Phys. Rev. Lett.* **94**, 058101 (2005).
 - [8] O. Kinouchi and M. Copelli, Optimal dynamical range of excitable networks at criticality, *Nat. Phys.* **2**, 348 (2006).
 - [9] W. L. Shew, H. Yang, T. Petermann, R. Roy, and D. Plenz, Neuronal avalanches imply maximum dynamic range in cortical networks at criticality, *J. Neurosci.* **29**, 15595 (2009).
 - [10] D. B. Larremore, W. L. Shew, and J. G. Restrepo, Predicting Criticality and Dynamic Range in Complex Networks: Effects of Topology, *Phys. Rev. Lett.* **106**, 058101 (2011).
 - [11] T. L. Ribeiro, M. Copelli, F. Caixeta, H. Belchior, D. R. Chialvo, M. A. Nicolelis, and S. Ribeiro, Spike avalanches exhibit universal dynamics across the sleep-wake cycle, *PLoS ONE* **5**, e14129 (2010).
 - [12] G. Hahn, A. Ponce-Alvarez, C. Monier, G. Benvenuti, A. Kumar, F. Chavane, G. Deco, and Y. Frégnac, Spontaneous cortical activity is transiently poised close to criticality, *PLoS Comput. Biol.* **13**, e1005543 (2017).
 - [13] A. J. Fontenele, N. A. P. de Vasconcelos, T. Feliciano, L. A. A. Aguiar, C. Soares-Cunha, B. Coimbra, L. Dalla Porta, S. Ribeiro, A. J. Rodrigues, N. Sousa *et al.*, Criticality between Cortical States, *Phys. Rev. Lett.* **122**, 208101 (2019).
 - [14] M. M. Steriade and R. W. McCarley, *Brainstem Control of Wakefulness and Sleep* (Springer Science & Business Media, New York, 2013).

- [15] N. Friedman, S. Ito, B. A. W. Brinkman, M. Shimono, R. E. L. DeVile, K. A. Dahmen, J. M. Beggs, and T. C. Butler, Universal Critical Dynamics in High Resolution Neuronal Avalanche Data, *Phys. Rev. Lett.* **108**, 208102 (2012).
- [16] J. Touboul and A. Destexhe, Power-law statistics and universal scaling in the absence of criticality, *Phys. Rev. E* **95**, 012413 (2017).
- [17] E. T. Jaynes, Information theory and statistical mechanics, *Phys. Rev.* **106**, 620 (1957).
- [18] E. Schneidman, M. J. Berry II, R. Segev, and W. Bialek, Weak pairwise correlations imply strongly correlated network states in a neural population, *Nature (London)* **440**, 1007 (2006).
- [19] G. Tkačik, T. Mora, O. Marre, D. Amodè, S. E. Palmer, M. J. Berry, and W. Bialek, Thermodynamics and signatures of criticality in a network of neurons, *Proc. Natl. Acad. Sci. USA* **112**, 11508 (2015).
- [20] T. Mora, S. Deny, and O. Marre, Dynamical Criticality in the Collective Activity of a Population of Retinal Neurons, *Phys. Rev. Lett.* **114**, 078105 (2015).
- [21] E. A. Clement, A. Richard, M. Thwaites, J. Ailon, S. Peters, and C. T. Dickson, Cyclic and sleep-like spontaneous alternations of brain state under urethane anaesthesia, *PLoS ONE* **3**, e2004 (2008).
- [22] A. Renart, J. de la Rocha, P. Bartho, L. Hollender, N. Parga, A. Reyes, and K. D. Harris, The asynchronous state in cortical circuits, *Science* **327**, 587 (2010).
- [23] K. D. Harris and A. Thiele, Cortical state and attention, *Nat. Rev. Neurosci.* **12**, 509 (2011).
- [24] N. A. De Vasconcelos, C. Soares-Cunha, A. J. Rodrigues, S. Ribeiro, and N. Sousa, Coupled variability in primary sensory areas and the hippocampus during spontaneous activity, *Sci. Rep.* **7**, 46077 (2017).
- [25] S. N. Kadir, D. F. Goodman, and K. D. Harris, High-dimensional cluster analysis with the masked EM algorithm, *Neural Comput.* **26**, 2379 (2014).
- [26] C. Rossant, S. N. Kadir, D. F. Goodman, J. Schulman, M. L. Hunter, A. B. Saleem, A. Grosmark, M. Belluscio, G. H. Denfield, A. S. Ecker *et al.*, Spike sorting for large, dense electrode arrays, *Nat. Neurosci.* **19**, 634 (2016).
- [27] Y. Senzai, A. Fernandez-Ruiz, and G. Buzsáki, Layer-specific physiological features and interlaminar interactions in the primary visual cortex of the mouse, *Neuron* **101**, 500 (2019).